Article

Stimuli-Responsive Naphthalene Diimide-Based Charge-Transfer Liquid Materials Showing Thermal Response to Tune Photoluminescent Properties

Takumi Omura [1,2], Shogo Morisako [1], and Kyosuke Isoda [1,*]

[1] Organic Materials Chemistry Group, Sagami Chemical Research Institute, 2743-1, Hayakawa, Ayase 252-1193, Kanagawa, Japan
[2] Division of Molecular Sciences, Graduate School of Science, Kitasato University, 1-15-1 Kitasato Minami-ku, Sagamihara 252-0373, Kanagawa, Japan
* Correspondence: k-isoda@sagami.or.jp; Tel.: +81-467-76-9264

Received: 16 April 2025; Revised: 26 May 2025; Accepted: 29 May 2025; Published: 3 June 2025

Abstract: Stimuli-responsive luminescent liquid materials have recently attracted considerable attention due to their potential to address the limitations of solid-state materials, such as the necessity of organic solvents and the difficulty in fabricating composite systems. Liquid-state materials offer superior processability and enable facile modulation of photophysical properties by simply selecting appropriate solutes. In particular, molecular designs incorporating electron-donating or electron-accepting properties into liquid materials allow to form charge-transfer (CT) complexes upon dissolving solutes with their opposite electronic properties, altering both solution color and photoluminescence (PL) behavior. In this study, we developed a room-temperature supercooled liquid material based on an electron-accepting naphthalene diimide (NADI) derivative, **BR-Val-NADI**. Upon dissolving electron-rich naphthalene-based derivatives (**NA-##s**) into **BR-Val-NADI**, **NA-##/BR-Val-NADI** with CT character were readily obtained as solutions, exhibiting various colors and PL properties. **NA-##/BR-Val-NADI** also functioned as printable PL inks that could be applied onto various substrates such as glass and paper. Notably, the PL properties of **NA-##/BR-Val-NADI** were responsive to thermal stimuli, with temperature-induced changes in PL color and PL off/on switching. These results highlight the potential of **NA-##/BR-Val-NADI** as a new class of stimuli-responsive soft materials for applications in printable photonic devices and smart sensing platforms.

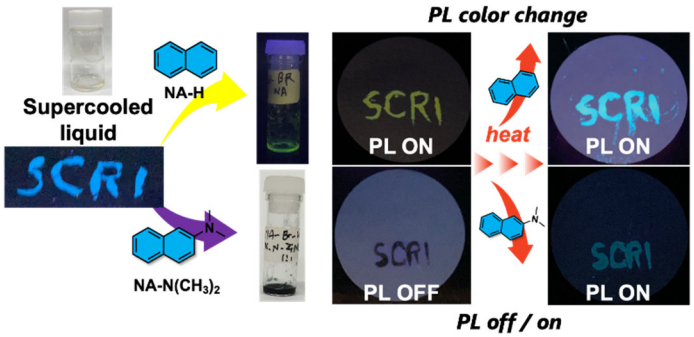

Keywords: naphthalene diimide; stimuli response; liquid material; stimuli-responsive liquid; photoluminescence

1. Introduction

Stimuli-responsive luminescent solid-state materials have been extensively reported and have emerged as a major research focus in materials science over the past two decades [1–10]. Molecular design strategies based on π-conjugated frameworks have been established for such materials, and research is underway not only on the development of novel compounds but also on their response to external stimuli and potential practical applications. However, these solid-state materials often require the use of volatile organic solvents during thin-film fabrication and precise molecular engineering techniques to avoid crystal polymorphism [11–13], which result in variations in luminescence colors in thin films. To address these challenges, the development of liquid-state materials has recently attracted growing attention, as they offer promising soft materials to overcome the limitations associated with solid-state systems [14–18].

Solvent-free liquid materials composed of π-conjugated frameworks are promising candidates for environmental-friendly soft materials [19–29]. Because these materials can be used under a wide range of conditions

without harmful volatile organic solvents, they present a sustainable alternative to conventional solid-state materials, of which applications align with some of the Sustainable Development Goals (SDGs) [30–32]. One of the key advantages of liquid materials lies in their ability to dissolve/disperse a wide variety of compounds such as organic and inorganic materials, enabling the facile preparation of composite materials [20,21,23,33–35]. For example, π-conjugated liquid materials with electron-accepting properties can readily dissolve electron-donating π-conjugated compounds, allowing for the straightforward preparation of charge-transfer (CT) solutions [20,36,37]. In contrast, the fabrication of composite solid-state materials typically requires complicated procedures such as co-crystallization or co-evaporation, which are both technically demanding and time-consuming. In this study, for the development of novel liquid materials in response to external stimuli, we focus on the liquification of 1,4,5,8-naphthalene diimide (NADI) framework.

NADI, a well-known rylene-based aromatic planar molecule, has attracted considerable attention due to its high thermal and photochemical stability, along with its intrinsic electronic and optical properties [38–40]. In particular, NADI exhibits high electron affinity and has been widely studied as an electron acceptor in CT complexes, both in the bulk state and in the dilute solution state in the field of supramolecular chemistry [38,39]. Recent studies have explored the incorporation of the NADI framework into macrocyclic molecules with host–guest interactions [41–45], covalent organic frameworks (COFs) [46–49], and n-type organic semiconductors [50–53]. Among these applications, the use of NADI-based materials for solid-state photoluminescence has drawn growing interest [39,54,55], however, their photoluminescent (PL) properties are often quenched due to strong molecular aggregation (aggregate-caused quenching (ACQ)) in the bulk state [56], which poses a significant challenge. To overcome this problem, various molecular design strategies have been reported, including the introduction of bulky substituents to suppress intermolecular interactions [57], the utilization of aggregation-induced enhanced emission (AIEE) properties [58–60], and the precise control of molecular packing. Despite the wide applicability of NADI derivatives, to the best of our knowledge, no reports have been reported on the liquefaction of NADI showing PL properties, except for one report on the preparation of the CT liquid composed of a supercooled-liquid NADI derivative [36].

In this study, we aimed to suppress the aggregation of the NADI core by introducing valine, a bulky amino acid with isopropyl side chains, during the imidization step, as well as by incorporating branched alkyl chains with large excluded volumes (Schemes 1 and 2). As a result, we obtained compound **BR-Val-NADI** exhibiting a supercooled liquid state at room temperature upon heating and subsequent cooling. Also, we found that **BR-Val-NADI** exhibits clear photoluminescence in its supercooled liquid state, whereas its luminescence is significantly reduced in the solid state. Notably, the emission color could be tuned by dissolving various π-conjugated naphthalene derivatives (**NA-##s**) via CT/exciplex formation. Also, their thermal stimuli enabled modulation of the PL properties. To the best of our knowledge, this represents the first report on the development of a PL NADI-based liquid material.

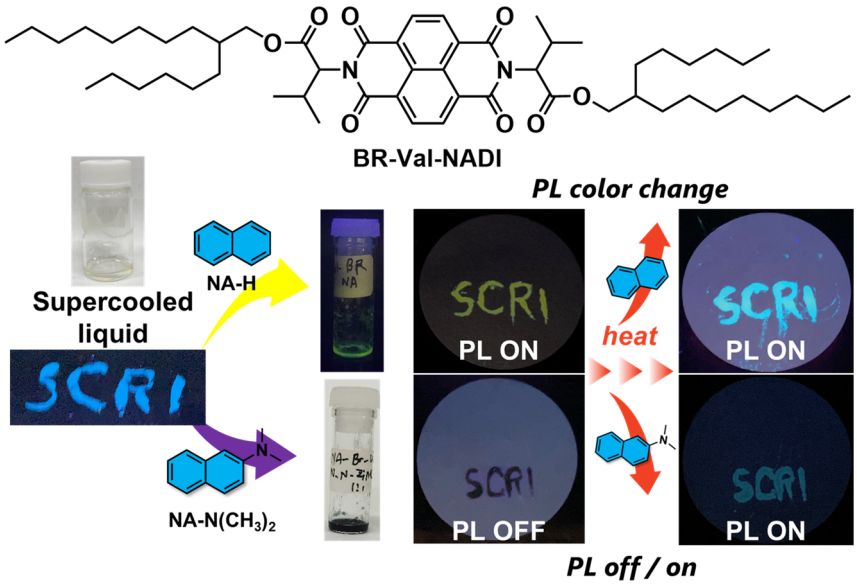

Scheme 1. Molecular structure of **BR-Val-NADI**, its photographs under room light and coated onto glass substrate under black light (365 nm), and photographs of thermal-responsive behaviors for **NA-H**/**BR-Val-NADI** and **NA-NMe$_2$**/**BR-Val-NADI** solutions under light and black light (365 nm).

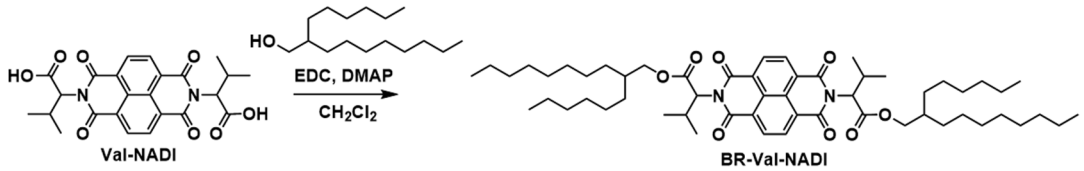

Scheme 2. Synthesis of **BR-Val-NADI.**

2. Materials and Methods

2.1. General Methods

The ^{1}H and ^{13}C NMR spectra were recorded on a Bruker AscendTM Avance III HD 400 MHz or UltraShield Plus 400 MHz NMR spectrometers (^{1}H: 400 MHz, ^{13}C: 101 MHz). All the spectroscopic measurements were carried out at room temperature. The chemical shifts of the ^{1}H and ^{13}C NMR signals are quoted relative to tetramethylsilane ($\delta = 0.00$) as internal standards. High-resolution atmospheric-pressure-chemical-ionization time-of-flight (HR-APCI-TOF-MS) mass spectra were collected on a Bruker compact QTOF spectrometer. UV-vis absorption spectra were recorded on a JASCO V-770 UV-vis spectrometer and the fluorescence spectra were recorded on a JASCO FP-8500 luminescence spectrophotometer. UV-vis and PL spectra were measured in thin films coated onto quartz glass substrates. DSC and TG-DTA measurements were performed on a Hitachi High-Tech EXSTAR6000 DSA6220 and Hitachi High-Tech EXSTAR6000 TG/DTA6200 at a scan rate of 10 °C min^{-1}. A OLYMPUS BX53M optical and polarizing optical microscope equipped with a Mettler FP90/82HT hot stage was used for visual observations of the optical textures. All reagents, all naphthalene derivatives, and solvents were purchased from FUJIFILM Wako Pure Chemical Co. (Osaka, Japan), Tokyo Chemical Industry Co., Ltd. (Tokyo, Japan), Kanto Chemical Co., Inc. (Tokyo, Japan), or Sigma Aldrich (St. Louis, MO, USA), and were used as received. **Val-NADI** was prepared according to previous reports [61].

2.2. Synthesis of **BR-Val-NADI**

To the CH_2Cl_2 (50 mL) solution of **Val-NADI** (3.50 g, 7.5 mmol), 2-hexyl-1-decanol (4.00 g, 16.5 mmol), 1-ethyl-3-(3-dimethylaminopropyl)carbodiimide hydrochloride (EDC, 3.16 g, 16.5 mmol), and 4-dimethylaminopyridine (DMAP, 4.58 g, 37.5 mmol) were added and stirred at room temperature for 2 days. After the addition of deionized water, the resulting mixture was extracted with $CHCl_3$ three times and the combined organic layer was dried over Na_2SO_4, filtered, and evaporated. The residual oil was purified by column chromatography (silica gel) with EtOAc/hexane (1/19) as the eluent to afford **BR-Val-NADI** (1.63 g, 23.8%) as a colorless waxy solid.

BR-Val-NADI: ^{1}H NMR (400 MHz, $CDCl_3$) δ 8.78 (s, 4H), 5.35 (d, J = 9.2 Hz, 2H), 4.10–3.97 (m, 4H), 2.93–2.82 (m, 2H), 1.59–1.49 (m, 2H), 1.33 (d, J = 7.1 Hz, 6H), 1.31–0.93 (m, 48H), 0.87 (t, J = 7.1 Hz, 6H), 0.80 (t, J = 7.4 Hz, 12H); $^{13}C\{^{1}H\}$ NMR (101 MHz, $CDCl_3$) δ 169.3, 162.5, 131.4, 126.8, 126.3, 68.1, 59.3, 37.1, 31.8, 31.7, 31.6, 31.3, 31.3, 29.9, 29.9, 29.5, 29.5, 29.4, 29.4, 29.3, 27.6, 26.6, 26.6, 26.5, 26.5, 22.6, 22.6, 22.1, 19.2, 14.1, 14.0; HRMS (APCI/TOF), m/z: Found: 915.6461 ([M+H]+), Calcd. for $C_{56}H_{86}N_2O_8$ ([M+H]+): 915.6457.

2.3. Computational Details

To obtain details of the electronic structure of **NA-#/BR-Val-NADI** complexes, computational studies were carried out by using the model compound **Val-NADI** instead of **BR-Val-NADI**. All calculations were performed in the gas phase using the Gaussian 16 program package (Rev. C.01) [62]. The ground-state geometry optimization of **NA-#/Val-NADI** was carried out with a B3LYP-D3(BJ) functional using 6-311+G(d,p) basis set [63]. After each geometry optimization, a frequency calculation at the same level was performed to verify that all the stationary points had no imaginary frequency. The time-dependent density functional theory (TD-DFT) [64,65] calculation was performed with a CAM-B3LYP-D3(BJ) functional using 6-311+G(d,p) basis set [66]. The results for TD-DFT calculations are summarized in Table S1. HOMO and LUMO levels for **NA-##s** and **Val-NADI** were calculated with a B3LYP-D3(BJ) functional using 6-31G (d,p) basis set.

2.4. Arrhenius Plot

TG diagrams obtained using the heating method can be analyzed by reaction kinetics theory [67]. The sublimation rate *v* follows an Arrhenius trend as

$$\frac{dm}{dt} = v = A\exp\left(-\frac{\Delta E}{RT}\right) f(m) \tag{1}$$

where m, A, ΔE, R, and T are mass loss rate, a pre-exponential factor, the activation energy, the universal real gas constant, and absolute temperature, respectively. $f(m)$ denotes $(1–m)^n$, and the parameter n is 1.0 when the sample is a supercooled liquid for **BR-Val-NADI** and a liquid for **BR-Val-PMDI**. Equation (1) can be rewritten as

$$\ln v - n\ln(1-m) = -\left(\frac{\Delta E}{R}\right)\frac{1}{T} + \ln A \tag{2}$$

The ΔE can be calculated from the slope of plots of $\ln v – n\ln(1–m)$ and $1/T$. Arrhenius plots of TG diagrams in Figure 1c was illustrated in Figure 1d by using the temperature range of vaporization for **BR-Val-NADI** and **BR-Val-PMDI**, where the values of ΔE were determined, respectively.

3. Results and Discussion

We investigated the fluidic behavior of **BR-Val-NADI** using differential scanning calorimetry (DSC) (Figure 1a). During the 1st heating, **BR-Val-NADI** exhibited a distinct endothermic peak derived from the melting. Upon the 1st cooling, no exothermic peak indicative of crystallization was observed corresponding to the endothermic peak observed on the 1st heating, whereas a glass transition (T_g) was observed at approximately −21 °C. Furthermore, the 2nd heating showed T_g similar to that upon the 1st cooling, however, the peak due to the post crystallization did not appear. Then, we conducted optical microscopy (OM) and polarized optical microscopy (POM) observations of **BR-Val-NADI** before and after melting by thermal treatment at 100 °C in Figure 1b. Before heating, **BR-Val-NADI** at room temperature showed a crystalline state with birefringence, whereas, after melting and subsequent cooling back to room temperature, no birefringence or crystalline features were observed. In addition, **BR-Val-NADI** could be used as an ink to be coated onto glass substrates and papers at room temperature, indicating that **BR-Val-NADI** adopts a room-temperature supercooled liquid state under ambient conditions.

It should be noted that T_g of **BR-Val-NADI** at −21 °C is higher than that of PMDI-based liquid material (**BR-Val-PMDI**) at −50 °C reported previously, which is composed of pyromellitic diimide core smaller p-conjugated framework than of **BR-Val-NADI** [20]. This increase in T_g suggests that **BR-Val-NADI** shows stronger intermolecular interactions, likely due to the expansion of the π-conjugated core as well as the influence on increase in the molecular weight compared to **BR-Val-PMDI**. It should be noted that the cold crystallization process was not observed during heating. Oguni et al. have reported that the supercooled liquid may have the crystal nucleation processes much lower than the glass transition temperature [68]. For **BR-Val-NADI**, the glass transition occurred prior to crystallization by branched alkyl chains suppressing the molecular ordering during the cooling. As a result, during heating, it presumably speculated that the phase transition from glass state to liquid state happened through no cold crystallization due to the molecular ordering. To evaluate the thermal stability of **BR-Val-NADI**, we performed the thermogravimetry-differential thermal analysis (TG-DTA) in Figure 1c. The TG trace of **BR-Val-NADI** showed a clearly single-step weight loss, indicating that **BR-Val-NADI** undergoes thermal evaporation without decomposition, which is an almost similar feature to **BR-Val-PMDI** [20]. Both of temperatures corresponding to 5 wt% and 100 wt% weight loss for **BR-Val-NADI** (365 °C and 433 °C) were higher than those of **BR-Val-PMDI** (318 °C and 416 °C), suggesting that the thermal durability of **BR-Val-NADI** should be improved. Furthermore, we estimated the activation energies ΔE due to the evaporation of both **BR-Val-NADI** and **BR-Val-PMDI** in Figure 1d from results of TG traces, of which values were calculated to be 171.1 kJ/mol for **BR-Val-NADI** and 113.4 kJ/mol for **BR-Val-PMDI**, respectively. These results are consistent with the observed T_g trends and suggest that the expanded π-conjugated core and the increase in molecular weight in **BR-Val-NADI** should enhance intermolecular interactions, contributing to its improved thermal and phase behavior.

To investigate the photophysical properties of **BR-Val-NADI** and its CT complexes, we measured the UV–vis absorption and PL spectra of **BR-Val-NADI** solutions containing various naphthalene derivatives as solutes in Figure 2. The solutions (**NA-##/BR-Val-NADI**) were prepared by dissolving **NA-##**s into **BR-Val-NADI** at a 1:1 molar ratio under heating, respectively. The UV–vis absorption spectrum of pure **BR-Val-NADI** exhibited a no characteristic peak in the long-wavelength range (Figure S1), whereas the **NA-##/BR-Val-NADI** showed new absorption bands at different wavelengths, distinct from that of **BR-Val-NADI** alone, indicating the formation of new electronic transitions (Figure 2a). In particular, **NA-NMe$_2$/BR-Val-NADI**, dissolving **NA-NMe$_2$** with the strongest electron-donating substituent, showed a new absorption peak at 620 nm, of which solution color is deep blue. To investigate the nature of this longer-wavelength peak observed in **NA-NMe$_2$/BR-Val-NADI**, time-dependent density functional theory (TD-DFT) calculations were performed using Gaussian 16 at the TD-CAM-

B3LYP-D3(BJ)/6-311+G(d,p) level of theory. For the calculation, a 1:1 complex of **NA-NMe$_2$** and **Val-NADI** instead of **BR-Val-NADI** was used (Figure 2). The TD-CAM-B3LYP functional was selected due to its long-range correction, making it suitable for modeling CT transitions. The TD-DFT results of 1:1 complex (**NA-NMe$_2$/Val-NADI**) revealed a low-energy absorption peak at 580 nm, which is almost consistent with the experimentally observed peak in the **NA-NMe$_2$/BR-Val-NADI** solution. The frontier molecular orbital analysis revealed that this transition is indicative of the electron transfer from the HOMO localized on **NA-NMe$_2$** as electron donor to the LUMO localized on **Val-NADI** as electron acceptor (Figure 2a). These results strongly support the assignment of the observed band as a CT transition from **NA-NMe$_2$** to **BR-Val-NADI**. In addition, TD-DFT calculations were performed for **NA-H/Val-NADI** and **NA-CN/Val-NADI**, which shows weaker electron-donating abilities compared to **NA-NMe$_2$**. In both cases, the calculations indicated the presence of CT transitions corresponding to HOMO–LUMO electron transfer, of which predicted CT bands appeared at shorter wavelengths than that of **NA-NMe$_2$**, consistent with their deeper HOMO levels. In the UV–vis absorption spectrum, **NA-H/BR-Val-NADI** showed a weak CT band. It is noteworthy that the position of the CT band was dependent on the HOMO levels of **NA-##**s. Peaks arising from the CT transition tend to undergo a bathochromically red-shift as the HOMO level of **NA-##**s becomes shallower, which correlates with a reduction in the energy gap between the HOMO level of **NA-##s** and the LUMO level of **BR-Val-NADI** (Figure S2). In contrast, solutions containing **NA-CN** and other electron-deficient derivatives (**NA-HCO** and **NA-COMe**) exhibit less CT bands than those with electron-donating **NA-##**s (Figure S3). This absence might be due to the weak donor ability of these compounds with electron-deficient substitutes and/or overlap between the expected CT bands and intrinsic absorption peaks of either **BR-Val-NADI** or **NA-##**s itself.

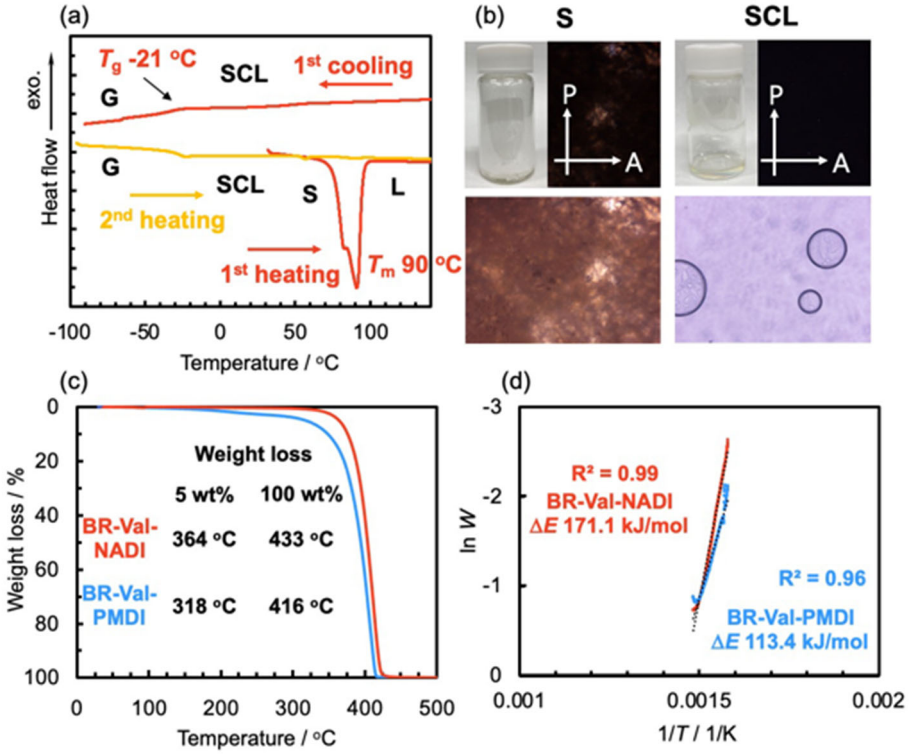

Figure 1. (**a**) DSC thermograms of **BR-Val-NADI** (red-colored lines: 1st heating and 1st cooling; orange-colored line: 2nd heating) at 10 K min^{-1}. S: solid state; L: liquid state; SCL: supercooled-liquid state; G: glassy state. (**b**) Photographs, polarized optical photomicrographs (POM) and optical photomicrographs (OM) of **BR-Val-NADI** in solid state (**left**) and supercooled-liquid state (**right**) at room temperature. S: solid state; SCL: supercooled-liquid state. Arrows indicate the directions of polarizer (P) and analyzer (A) axes. **BR-Val-NADI** in the solid state was obtained after purification through column chromatography, evaporation from hexane/ethyl acetate, and drying under vacuum. (**c**) TG analysis of **BR-Val-NADI** and **BR-Val-PMDI** over the temperature range from 25 to 500 °C under N_2 atmosphere with their temperatures at 5 wt% and 100 wt% weight loss. (**d**) Temperature dependence for weight loss due to vaporization process of **BR-Val-NADI** and **BR-Val-PMDI** (ln$W$ vs. T^{-1}) at 10 K min^{-1} heating rate under static N_2 atmosphere. These plots correspond to the range of weight loss of **BR-Val-NADI** and **BR-Val-PMDI** in TG traces. The values shown in the figure indicate activation energies of **BR-Val-NADI** and **BR-Val-PMDI**, respectively.

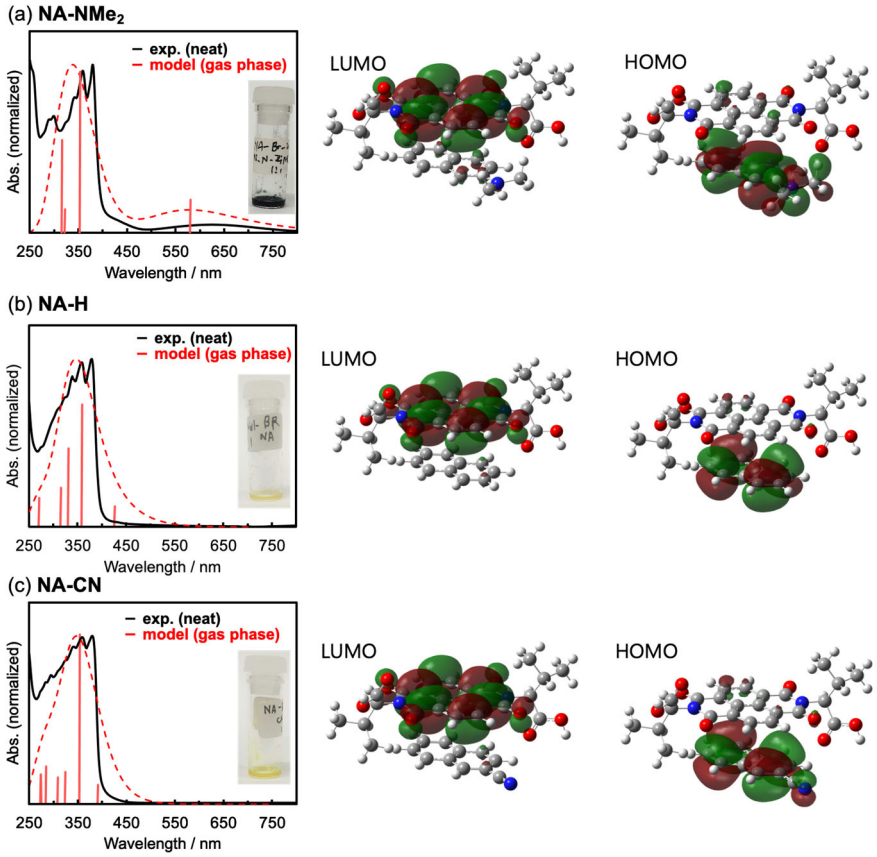

Figure 2. Experimental (neat) and simulated (gas) UV-vis absorption spectra and frontier orbitals based on TD-DFT calculations (TD-CAM-B3LYP-D3(BJ)/6-311+G(d,p)) for (**a**) NA-NMe_2/BR-Val-NADI and **NA-NMe_2/Val-NADI**, (**b**) **NA-H/BR-Val-NADI** and **NA-H/Val-NADI**, and (**c**) **NA-CN/BR-Val-NADI** and **NA-CN/Val-NADI**.

Next, we investigated the PL properties of the **BR-Val-NADI**-based solutions in Figures 3a,b, S2 and S3. In its supercooled-liquid state, **BR-Val-NADI** exhibited sky-blue emission with a peak at 481 nm, which is distinctly different from its solid state showing less emission (Figures 3b and S1). Upon dissolving **NA-H** into **BR-Val-NADI**, the resulting solution **NA-H/BR-Val-NADI** exhibited yellow emission with a PL peak at 550 nm. Furthermore, varying the substituents introduced into **NA-##**s could tune the emission colors. For instance, **NA-##**s (**NA-CN**, **NA-HCO** and **NA-COMe**) bearing electron-withdrawing groups exhibited blue-shifted PL peaks compared to **NA-H**, while those (**NA-Me**) with electron-donating substituents showed red-shifted emissions, with the appearance of peaks at longer wavelengths than **NA-H**. To understand these trends, we examined the correlation between the observed PL emission peaks and the HOMO levels of **NA-##**s by DFT calculations (Figure 3c). The results revealed a clear trend: as the HOMO level becomes shallower (i.e., higher in energy), the emission peaks shifts toward the bathochromic region, indicating a stronger CT interaction.

Finally, we investigated the thermal responsiveness of **NA-##/BR-Val-NADI** (Figure 4). Given that **NA-##**s are known to volatilize upon heating [69,70], we hypothesized that selective evaporation of the **NA-##** component from **NA-##/BR-Val-NADI** could modulate the emission properties. When a filter paper coated with **NA-H/BR-Val-NADI** was observed under UV light (365 nm), it emitted yellow fluorescence similar to the original solution (Figure 4). After heating the coated paper at 150 °C for 5 min, the emission color changed from yellow to sky-blue. This change indicates the evaporation of **NA-H**, leaving behind **BR-Val-NADI**, which emits sky-blue fluorescence. In contrast, **NA-NMe_2/BR-Val-NADI**, which initially exhibited no emission, could emit sky-blue fluorescence after heating at 150 °C for 5 min by the evaporation of **NA-NMe_2** only. These findings suggest that **NA-##/BR-Val-NADI** systems can function as thermal-responsive liquid materials, enabling tunable PL color changes or PL OFF/ON switching of emission through thermal stimuli.

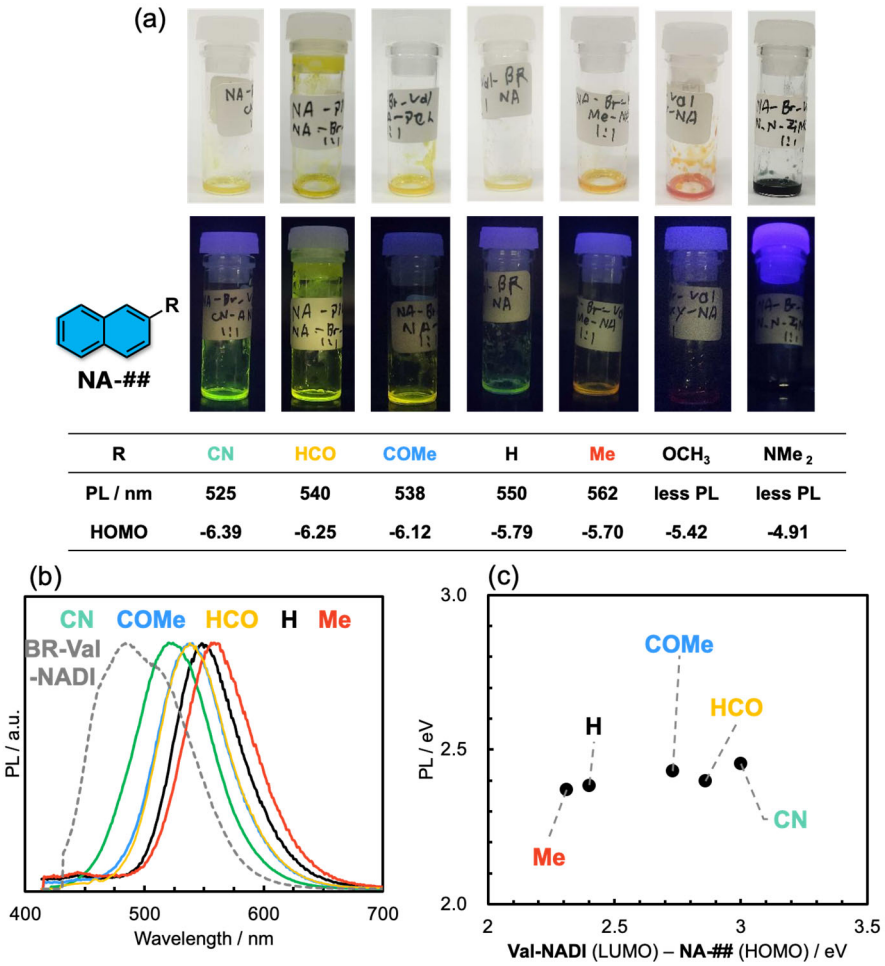

R	CN	HCO	COMe	H	Me	OCH_3	NMe_2
PL / nm	525	540	538	550	562	less PL	less PL
HOMO	-6.39	-6.25	-6.12	-5.79	-5.70	-5.42	-4.91

Figure 3. (**a**) Photographs of **NA-##/BR-Val-NADI** under 365 nm light. (**b**) PL spectra of **NA-##/BR-Val-NADI** in a neat state. (**c**) The relationship between peaks in PL spectra and HOMO-LUMO gap estimated by DFT calculations with a B3LYP-D3(BJ) functional using 6-31G (d,p) basis set.

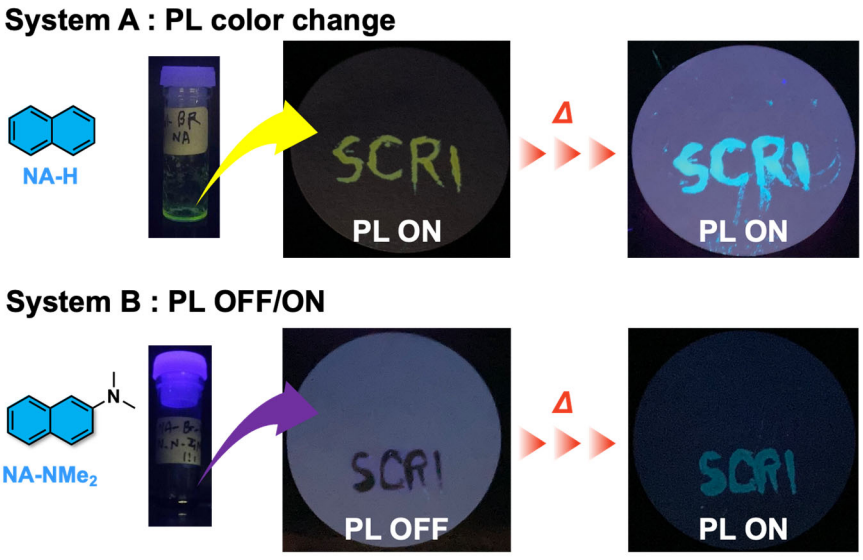

Figure 4. Thermal-responsive behaviors of **NA-H/BR-Val-NADI** in PL color change for system A and **NA-NMe_2/BR-Val-NADI** in PL color change for system B.

4. Conclusions

We successfully synthesized a room-temperature supercooled liquid material based on an electron-accepting naphthalene diimide derivative, **BR-Val-NADI**. By dissolving **NA-##**s, **NA-##/BR-Val-NADI** can be readily

obtained as CT-type liquid solutions, that exhibited tunable colors and distinct PL properties. **NA-##/BR-Val-NADI** also demonstrated excellent printability, enabling their application as PL inks on various substrates such as glass and paper. Also, the PL characteristics of **NA-##/BR-Val-NADI** were highly responsive to thermal stimuli, including temperature-dependent color change and PL off/on switching. These findings underscore the promise of **NA-##/BR-Val-NADI** systems as a new class of thermos-responsive soft materials with potential for use in printable photonic devices and smart sensing technologies.

Supplementary Materials: The following supporting information can be downloaded at: https://media.sciltp.com/articles/others/250604170835175 8/MI-1043-SI-final.pdf, Figure S1: Photographs of **BR-Val-NADI** under room light and under 365 nm light. SCL: supercooled liquid; S: solid. The UV-vis absorption and PL spectra of **BR-Val-NADI** in supercooled-liquid state; Figure S2. The UV-vis absorption (left) and PL (right) spectra of **NA-H/BR-Val-NADI**, **NA-Me/BR-Val-NADI**, **NA-OMe/BR-Val-NADI**, and **NA-NMe$_2$/BR-Val-NADI** in solution states. Photographs of solutions under room light and under 365 nm light. Arrows indicate CT peaks; Figure S3. The UV-vis absorption (left) and PL (right) spectra of **NA-CN/BR-Val-NADI**, **NA-HCO/BR-Val-NADI**, and **NA-COMe/BR-Val-NADI**, in solution states. Photographs of solutions under room light and under 365 nm light; Table S1. Calculated wavelengths for the absorption spectrum of (a) **NA-NMe$_2$/Val-NADI**, (b) **NA-H/Val-NADI**, and (c) **NA-CN/Val-NADI** complexes, their oscillator strengths (>0.02), and the associated transitions with |CI coefficient| > 0.2.

Author Contributions: T.O. synthesized **BR-Val-NADI** and carries out experiments. S.M. carried out the DFT calculation and experiments. K.I. de-signed and supervised this project and wrote the manuscript. All authors have read and agreed to the published version of the manuscript.

Funding: This work was supported by the Japan Society for the Promotion of Science (JSPS) KAKENHI Grant Numbers 22K05257 (K.I.), 25K08603 (K.I.), 23K13727 (S.M.), and 25K08617 (S.M.) and Iketani Science and Technology Foundation (K.I.), Kato Foundation for Promotion of Science (K.I.), and Tokyo Ohka Foundation for The Promotion of Science and Technology (K.I.).

Data Availability Statement: The data that support the findings of this study are available from the corresponding author upon reasonable request.

Conflicts of Interest: The authors declare no conflict of interest.

References

1. Yerushalmi, R.; Scherz, A.; van der Boom, M.E.; Kraatz, H.-B. Stimuli responsive materials: New avenues toward smart organic devices. *J. Mater. Chem.* **2005**, *15*, 4480–4487. https://doi.org/10.1039/B505212B.
2. Huang, Y.; Ning, L.; Zhang, X.; Zhou, Q.; Gong, Q.; Zhang, Q. Stimuli-fluorochromic smart organic materials. *Chem. Soc. Rev.* **2024**, *53*, 1090–1166. https://doi.org/10.1039/D2CS00976E.
3. Yan, D.; Wang, Z.; Zhang, Z. Stimuli-Responsive Crystalline Smart Materials: From Rational Design and Fabrication to Applications. *Acc. Chem. Res.* **2022**, *55*, 1047–1058. https://doi.org/10.1021/acs.accounts.2c00027.
4. Sun, H.; Shen, S.; Li, C.; Yu, W.; Xie, Q.; Wu, D.; Zhu, L. Stimuli-Responsive Dual-Emission Property of Single-Luminophore-Based Materials. *Adv. Funct. Mater.* **2025**, *35*, 2415400. https://doi.org/10.1002/adfm.202415400.
5. Wu, W.; Chen, K.; Wang, T.; Wang, N.; Huang, X.; Zhou, L.; Wang, Z.; Hao, H. Stimuli-responsive flexible organic crystals. *J. Mater. Chem. C* **2023**, *11*, 2026–2052. https://doi.org/10.1039/D2TC04642C.
6. Huang, L.; Qian, C.; Ma, Z. Stimuli-Responsive Purely Organic Room-Temperature Phosphorescence Materials. *Chem.-Eur. J.* **2020**, *26*, 11914–11930. https://doi.org/10.1002/chem.202000526.
7. Karunakar, K.K.; Cheriyan, B.V.; Anandakumar, R.; Murugathirumal, A.; Kataria, K.; Yabase, L. Stimuli-Responsive Smart Materials: Bridging the Gap Between Biotechnology and Regenerative Medicine. *Bioprinting* **2025**, *48*, e00415. https://doi.org/10.1016/j.bprint.2025.e00415.
8. Zhao, J.; Du, J.; Qin, T.; Zhang, S.X.-A.; Sheng, L. "Confined Eutectic" Strategy for Visual Refrigeration Responsive Fluorescent Materials with Easy Preparation and Multi-Color Tunability. *Adv. Sci.* **2025**, 2503779. https://doi.org/10.1002/advs.202503779.
9. Du, J.; Sheng, L.; Xu, Y.; Chen, Q.; Gu, C.; Li, M.; Zhang, S.X.-A. Printable Off-On Thermoswitchable Fluorescent Materials for Programmable Thermally Controlled Full-Color Displays and Multiple Encryption. *Adv. Mater.* **2021**, *33*, 2008055. https://doi.org/10.1002/adma.202008055.
10. Du, J.; Sheng, L.; Chen, Q.; Xu, Y.; Li, W.; Wang, X.; Li, M.; Zhang, S.X.-A. Simple and general platform for highly adjustable thermochromic fluorescent materials and multi-feasible applications. *Mater. Horiz.* **2019**, *6*, 1654–1662. https://doi.org/10.1039/C9MH00253G.
11. Davey, R.J.; Schroeder, S.L.M.; ter Horst, J.H. Nucleation of Organic Crystals—A Molecular Perspective. *Angew. Chem. Int. Ed.* **2013**, *52*, 2166–2179. https://doi.org/10.1002/anie.201204824.
12. Liang, C. Organic Polymorphs Based on AIE-Active Molecules: Preparation, Characterization, and Application. *Cryst. Growth Des.* **2024**, *24*, 7322–7341. https://doi.org/10.1021/acs.cgd.4c00499.

13. Chung, H.; Diao, Y. Polymorphism as an emerging design strategy for high performance organic electronics. *J. Mater. Chem. C* **2016**, *4*, 3915–3933. https://doi.org/10.1039/C5TC04390E.
14. Nakanishi, T. (Ed.) *Functional Organic Liquids*; John Wiley & Sons: Hoboken, NJ, USA, 2019; pp. i–xii.
15. Ghosh, A.; Nakanishi, T. Frontiers of solvent-free functional molecular liquids. *Chem. Commum.* **2017**, *53*, 10344–10357. https://doi.org/10.1039/C7CC05883G.
16. Tateyama, A.; Nakanishi, T. Responsive molecular liquid materials. *Responsive Mater.* **2023**, *1*, e20230001. https://doi.org/10.1002/rpm.20230001.
17. Lu, F.; Nakanishi, T. Solvent-Free Luminous Molecular Liquids. *Adv. Opt. Mater.* **2019**, *7*, 1900176. https://doi.org/10.1002/adom.201900176.
18. Wakchaure, V.C.; Channareddy, G.; Babu, S.S. Solvent-Free Organic Liquids: An Efficient Fluid Matrix for Unexplored Functional Hybrid Materials. *Acc. Chem. Res.* **2024**, *57*, 670–684. https://doi.org/10.1021/acs.accounts.3c00670.
19. Tateyama, A.; Nagura, K.; Yamanaka, M.; Nakanishi, T. Alkyl–π Functional Molecular Gels: Control of Elastic Modulus and Improvement of Electret Performance. *Angew. Chem. Int. Ed.* **2024**, *63*, e202402874. https://doi.org/10.1002/anie.202402874.
20. Omura, T.; Morisako, S.; Isoda, K. Amino acid-appended pyromellitic diimide liquid materials, their photoluminescence, and thermal response turning photoluminescence off. *Chem. Commum.* **2024**, *60*, 9352–9355. https://doi.org/10.1039/D4CC02229G.
21. Ogoshi, T.; Azuma, S.; Wada, K.; Tamura, Y.; Kato, K.; Ohtani, S.; Kakuta, T.; Yamagishi, T.-A. Exciplex Formation by Complexation of an Electron-Accepting Guest in an Electron-Donating Pillar [5] arene Host Liquid. *J. Am. Chem. Soc.* **2024**, *146*, 9828–9835. https://doi.org/10.1021/jacs.3c14582.
22. Xu, Z.; Wang, Z.; Yao, W.; Gao, Y.; Li, Y.; Shi, H.; Huang, W.; An, Z. Supercooled Liquids with Dynamic Room Temperature Phosphorescence Using Terminal Hydroxyl Engineering. *Angew. Chem. Int. Ed.* **2023**, *62*, e202301564. https://doi.org/10.1002/anie.202301564.
23. Tanabe, Y.; Tsutsui, H.; Matsuda, S.; Shikita, S.; Yasuda, T.; Isoda, K. Pyromellitic-Diimide-Based Liquid Material Forming an Exciplex with Naphthalene. *ChemPhotoChem* **2023**, *7*, e202200287. https://doi.org/10.1002/cptc.202200287.
24. Sato, Y.; Mutoh, Y.; Morishita, S.; Tsurumachi, N.; Isoda, K. Stimulus-Responsive Supercooled π-Conjugated Liquid and Its Application in Rewritable Media. *J. Phys. Chem. Lett.* **2021**, *12*, 3014–3018. https://doi.org/10.1021/acs.jpclett.1c00247.
25. Ikenaga, A.; Akiyama, Y.; Ishiyama, T.; Gon, M.; Tanaka, K.; Chujo, Y.; Isoda, K. Stimuli-Responsive Self-Assembly of π-Conjugated Liquids Triggers Circularly Polarized Luminescence. *ACS Appl. Mater. Interfaces* **2021**, *13*, 47127–47133. https://doi.org/10.1021/acsami.1c13119.
26. Isoda, K.; Matsubara, M.; Ikenaga, A.; Akiyama, Y.; Mutoh, Y. Reversibly/irreversibly stimuli-responsive inks based on N-heteroacene liquids. *J. Mater. Chem. C* **2019**, *7*, 14075–14079. https://doi.org/10.1039/C9TC05195C.
27. Isoda, K.; Ishiyama, T.; Mutoh, Y.; Matsukuma, D. Stimuli-Responsive Room-Temperature N-Heteroacene Liquid: In Situ Observation of the Self-Assembling Process and Its Multiple Properties. *ACS Appl. Mater. Interfaces* **2019**, *11*, 12053–12062. https://doi.org/10.1021/acsami.8b21695.
28. Giri, N.; Del Pópolo, M.G.; Melaugh, G.; Greenaway, R.L.; Rätzke, K.; Koschine, T.; Pison, L.; Gomes, M.F.C.; Cooper, A.I.; James, S.L. Liquids with permanent porosity. *Nature* **2015**, *527*, 216–220. https://doi.org/10.1038/nature16072.
29. Chung, K.; Kwon, M.S.; Leung, B.M.; Wong-Foy, A.G.; Kim, M.S.; Kim, J.; Takayama, S.; Gierschner, J.; Matzger, A.J.; Kim, J. Shear-Triggered Crystallization and Light Emission of a Thermally Stable Organic Supercooled Liquid. *ACS Cent. Sci.* **2015**, *1*, 94–102. https://doi.org/10.1021/acscentsci.5b00091.
30. Clarke, C.J.; Tu, W.-C.; Levers, O.; Bröhl, A.; Hallett, J.P. Green and Sustainable Solvents in Chemical Processes. *Chem. Rev.* **2018**, *118*, 747–800. https://doi.org/10.1021/acs.chemrev.7b00571.
31. Horváth, I.T. Introduction: Sustainable Chemistry. *Chem. Rev.* **2018**, *118*, 369–371. https://doi.org/10.1021/acs.chemrev.7b00721.
32. Ghosh, A.; Yoshida, M.; Suemori, K.; Isago, H.; Kobayashi, N.; Mizutani, Y.; Kurashige, Y.; Kawamura, I.; Nirei, M.; Yamamuro, O.; et al. Soft chromophore featured liquid porphyrins and their utilization toward liquid electret applications. *Nat. Commun.* **2019**, *10*, 4210. https://doi.org/10.1038/s41467-019-12249-8.
33. Goudappagouda; Manthanath, A.; Wakchaure, V.C.; Ranjeesh, K.C.; Das, T.; Vanka, K.; Nakanishi, T.; Babu, S.S. Paintable Room-Temperature Phosphorescent Liquid Formulations of Alkylated Bromonaphthalimide. *Angew. Chem. Int. Ed.* **2019**, *58*, 2284–2288. https://doi.org/10.1002/anie.201811834.
34. Santhosh Babu, S.; Aimi, J.; Ozawa, H.; Shirahata, N.; Saeki, A.; Seki, S.; Ajayaghosh, A.; Möhwald, H.; Nakanishi, T. Solvent-Free Luminescent Organic Liquids. *Angew. Chem. Int. Ed.* **2012**, *51*, 3391–3395. https://doi.org/10.1002/anie.201108853.
35. Babu, S.S.; Hollamby, M.J.; Aimi, J.; Ozawa, H.; Saeki, A.; Seki, S.; Kobayashi, K.; Hagiwara, K.; Yoshizawa, M.; Möhwald, H.; et al. Nonvolatile liquid anthracenes for facile full-colour luminescence tuning at single blue-light excitation. *Nat. Commun.* **2013**, *4*, 1969. https://doi.org/10.1038/ncomms2969.

36. Wakchaure, V.C.; Pillai, L.V.; Goudappagouda; Ranjeesh, K.C.; Chakrabarty, S.; Ravindranathan, S.; Rajamohanan, P.R.; Babu, S.S. Charge transfer liquid: A stable donor–acceptor interaction in the solvent-free liquid state. *Chem. Commum.* **2019**, *55*, 9371–9374. https://doi.org/10.1039/C9CC03671G.
37. Iguchi, H.; Furutani, H.; Kimizuka, N. Ionic Charge-Transfer Liquid Crystals Formed by Alternating Supramolecular Copolymerization of Liquid π-Donors and TCNQ. *Front. Chem.* **2021**, *9*, 657246. https://doi.org/10.3389/fchem.2021.657246.
38. Al Kobaisi, M.; Bhosale, S.V.; Latham, K.; Raynor, A.M.; Bhosale, S.V. Functional Naphthalene Diimides: Synthesis, Properties, and Applications. *Chem. Rev.* **2016**, *116*, 11685–11796. https://doi.org/10.1021/acs.chemrev.6b00160.
39. Bhosale, S.V.; Jani, C.H.; Langford, S.J. Chemistry of naphthalene diimides. *Chem. Soc. Rev.* **2008**, *37*, 331–342. https://doi.org/10.1039/B615857A.
40. Langford, S.J.; Latter, M.J.; Woodward, C.P. Progress in Charge Transfer Systems Utilizing Porphyrin Donors and Simple Aromatic Diimide Acceptor Units. *Photochem. Photobiol.* **2006**, *82*, 1530–1540. https://doi.org/10.1111/j.1751-1097.2006.tb09808.x.
41. Wang, Y.; Wu, H.; Stoddart, J.F. Molecular Triangles: A New Class of Macrocycles. *Acc. Chem. Res.* **2021**, *54*, 2027–2039. https://doi.org/10.1021/acs.accounts.1c00108.
42. Hartmann, D.; Penty, S.E.; Zwijnenburg, M.A.; Pal, R.; Barendt, T.A. A Bis-Perylene Diimide Macrocycle Chiroptical Switch. *Angew. Chem. Int. Ed.* **2025**, *64*, e202501122. https://doi.org/10.1002/anie.202501122.
43. Tominaga, M.; Kawahata, M.; Itoh, T.; Yamaguchi, K. Spherical Aggregates and Crystal Structure of Naphthalenediimide-Based Macrocycle and Complexation with Perylene. *Cryst. Growth Des.* **2018**, *18*, 37–41. https://doi.org/10.1021/acs.cgd.7b01361.
44. Beldjoudi, Y.; Narayanan, A.; Roy, I.; Pearson, T.J.; Cetin, M.M.; Nguyen, M.T.; Krzyaniak, M.D.; Alsubaie, F.M.; Wasielewski, M.R.; Stupp, S.I.; et al. Supramolecular Tessellations by a Rigid Naphthalene Diimide Triangle. *J. Am. Chem. Soc.* **2019**, *141*, 17783–17795. https://doi.org/10.1021/jacs.9b08758.
45. Ling, Q.-H.; Zhu, J.-L.; Qin, Y.; Xu, L. Naphthalene diimide- and perylene diimide-based supramolecular cages. *Mater. Chem. Front.* **2020**, *4*, 3176–3189. https://doi.org/10.1039/D0QM00540A.
46. Jhulki, S.; Feriante, C.H.; Mysyk, R.; Evans, A.M.; Magasinski, A.; Raman, A.S.; Turcheniuk, K.; Barlow, S.; Dichtel, W.R.; Yushin, G.; et al. A Naphthalene Diimide Covalent Organic Framework: Comparison of Cathode Performance in Lithium-Ion Batteries with Amorphous Cross-linked and Linear Analogues, and Its Use in Aqueous Lithium-Ion Batteries. *ACS Appl. Energy Mater.* **2021**, *4*, 350–356. https://doi.org/10.1021/acsaem.0c02281.
47. van der Jagt, R.; Vasileiadis, A.; Veldhuizen, H.; Shao, P.; Feng, X.; Ganapathy, S.; Habisreutinger, N.C.; van der Veen, M.A.; Wang, C.; Wagemaker, M.; et al. Synthesis and Structure–Property Relationships of Polyimide Covalent Organic Frameworks for Carbon Dioxide Capture and (Aqueous) Sodium-Ion Batteries. *Chem. Mater.* **2021**, *33*, 818–833. https://doi.org/10.1021/acs.chemmater.0c03218.
48. Wang, L.-L.; Ni, X.-Q.; Han, Y.-J.; Zhang, J.; Luo, H.-B.; Qiao, Q.; Wu, Y.-P.; Ren, X.-M. Acidified naphthalene diimide covalent organic frameworks with superior proton conduction for solid-state proton batteries. *J. Mater. Chem. C* **2025**, *13*, 4398–4404. https://doi.org/10.1039/D4TC04322G.
49. Huang, Z.; Zhang, Y.; Zhao, S.; Xu, Y.; Qi, X.; Zhang, L.; Zhao, Y. Two-dimensional covalent organic frameworks with spatial-distribution defined D-A structures for efficient near-infrared photothermal conversion. *Microporous Mesoporous Mater.* **2022**, *343*, 112191. https://doi.org/10.1016/j.micromeso.2022.112191.
50. Katz, H.E.; Johnson, J.; Lovinger, A.J.; Li, W. Naphthalenetetracarboxylic Diimide-Based n-Channel Transistor Semiconductors: Structural Variation and Thiol-Enhanced Gold Contacts. *J. Am. Chem. Soc.* **2000**, *122*, 7787–7792. https://doi.org/10.1021/ja000870g.
51. Katz, H.E.; Lovinger, A.J.; Johnson, J.; Kloc, C.; Siegrist, T.; Li, W.; Lin, Y.Y.; Dodabalapur, A. A soluble and air-stable organic semiconductor with high electron mobility. *Nature* **2000**, *404*, 478–481. https://doi.org/10.1038/35006603.
52. He, T.; Stolte, M.; Burschka, C.; Hansen, N.H.; Musiol, T.; Kälblein, D.; Pflaum, J.; Tao, X.; Brill, J.; Würthner, F. Single-crystal field-effect transistors of new Cl_2-NDI polymorph processed by sublimation in air. *Nat. Commun.* **2015**, *6*, 5954. https://doi.org/10.1038/ncomms6954.
53. Kao, C.-C.; Lin, P.; Shen, Y.-Y.; Yan, J.-Y.; Ho, J.-C.; Lee, C.-C.; Chan, L.-H. Solid-state structure of the naphthalene-based n-type semiconductor, and performance improved with Mo-based source/drain electrodes. *Synth. Met.* **2008**, *158*, 299–305. https://doi.org/10.1016/j.synthmet.2008.01.019.
54. Basak, S.; Nandi, N.; Paul, S.; Banerjee, A. Luminescent Naphthalene Diimide-Based Peptide in Aqueous Medium and in Solid State: Rewritable Fluorescent Color Code. *ACS Omega* **2018**, *3*, 2174–2182. https://doi.org/10.1021/acsomega.7b01813.
55. Sakai, N.; Mareda, J.; Vauthey, E.; Matile, S. Core-substituted naphthalenediimides. *Chem. Commum.* **2010**, *46*, 4225–4237. https://doi.org/10.1039/C0CC00078G.

56. Yuan, W.Z.; Lu, P.; Chen, S.; Lam, J.W.Y.; Wang, Z.; Liu, Y.; Kwok, H.S.; Ma, Y.; Tang, B.Z. Changing the Behavior of Chromophores from Aggregation-Caused Quenching to Aggregation-Induced Emission: Development of Highly Efficient Light Emitters in the Solid State. *Adv. Mater.* **2010**, *22*, 2159–2163. https://doi.org/10.1002/adma.200904056.
57. Pervin, R.; Manian, A.; Chen, Z.; Christofferson, A.J.; Owyong, T.C.; Bradley, S.J.; White, J.M.; Ghiggino, K.P.; Russo, S.P.; Wong, W.W.H. Medium effects on the fluorescence of Imide-substituted naphthalene diimides. *J. Photochem. Photobiol. A* **2023**, *436*, 114364. https://doi.org/10.1016/j.jphotochem.2022.114364.
58. Hong, Y.; Lam, J.W.Y.; Tang, B.Z. Aggregation-induced emission. *Chem. Soc. Rev.* **2011**, *40*, 5361–5388. https://doi.org/10.1039/C1CS15113D.
59. Molla, M.R.; Ghosh, S. Aqueous self-assembly of chromophore-conjugated amphiphiles. *Phys. Chem. Chem. Phys.* **2014**, *16*, 26672–26683. https://doi.org/10.1039/C4CP03791J.
60. Lasitha, P.; Prasad, E. Orange red emitting naphthalene diimide derivative containing dendritic wedges: Aggregation induced emission (AIE) and detection of picric acid (PA). *RSC Adv.* **2015**, *5*, 41420–41427. https://doi.org/10.1039/C5RA04857E.
61. Mollick, S.; Mukherjee, S.; Kim, D.; Qiao, Z.; Desai, A.V.; Saha, R.; More, Y.D.; Jiang, J.; Lah, M.S.; Ghosh, S.K. Hydrophobic Shielding of Outer Surface: Enhancing the Chemical Stability of Metal–Organic Polyhedra. *Angew. Chem. Int. Ed.* **2019**, *58*, 1041–1045. https://doi.org/10.1002/anie.201811037.
62. Frisch, M.J.; Trucks, G.W.; Schlegel, H.B.; Scuseria, G.E.; Robb, M.A.; Cheeseman, J.R.; Scalmani, G.; Barone, V.; Petersson, G.A.; et al. *Gaussian 16, Revision C.01*; Gaussian, Inc.: Wallingford, CT, USA, 2019.
63. Grimme, S.; Ehrlich, S.; Goerigk, L. Effect of the damping function in dispersion corrected density functional theory. *J. Comput. Chem.* **2011**, *32*, 1456–1465. https://doi.org/10.1002/jcc.21759.
64. Bauernschmitt, R.; Ahlrichs, R. Treatment of electronic excitations within the adiabatic approximation of time dependent density functional theory. *Chem. Phys. Lett.* **1996**, *256*, 454–464. https://doi.org/10.1016/0009-2614(96)00440-X.
65. Casida, M.E.; Jamorski, C.; Casida, K.C.; Salahub, D.R. Molecular excitation energies to high-lying bound states from time-dependent density-functional response theory: Characterization and correction of the time-dependent local density approximation ionization threshold. *J. Chem. Phys.* **1998**, *108*, 4439–4449. https://doi.org/10.1063/1.475855.
66. Yanai, T.; Tew, D.P.; Handy, N.C. A new hybrid exchange–correlation functional using the Coulomb-attenuating method (CAM-B3LYP). *Chem. Phys. Lett.* **2004**, *393*, 51–57. https://doi.org/10.1016/j.cplett.2004.06.011.
67. Chirico, R.D.; Knipmeyer, S.E.; Nguyen, A.; Steele, W.V. The thermodynamic properties to the temperature 700 K of naphthalene and of 2,7-dimethylnaphthalene. *J. Chem. Thermodyn.* **1993**, *25*, 1461–1494. https://doi.org/10.1006/jcht.1993.1148.
68. Okamoto, N.; Oguni, M. Discovery of crystal nucleation proceeding much below the glass transition temperature in a supercooled liquid. *Solid State Commun.* **1996**, *99*, 53–56. https://doi.org/10.1016/0038-1098(96)00139-1.
69. Dai, J.; McKee, M.L.; Samokhvalov, A. Adsorption of naphthalene and indole on F300 MOF in liquid phase by the complementary spectroscopic, kinetic and DFT studies. *J. Porous Mater.* **2014**, *21*, 709–727. https://doi.org/10.1007/s10934-014-9818-3.
70. Berlman, I.B.; Weinreb, A. On the fluorescence spectrum and decay time of naphthalene. *Mol. Phys.* **1962**, *5*, 313–319. https://doi.org/10.1080/00268976200100351.